YTHDF1 Promotes Gastric Carcinogenesis by Controlling Translation of *FZD7*

Jingnan Pi[1,2], Wen Wang[1,2], Ming Ji[3], Xiaoshuang Wang[1,2], Xueju Wei[1,2], Jing Jin[3], Tao Liu[4], Jiaqi Qiang[1,2], Zhihong Qi[5], Feng Li[6], Yue Liu[1,2], Yanni Ma[1,2], Yanmin Si[1,2], Yue Huo[1,2], Yufeng Gao[1,2], Yiying Chen[1,2], Lei Dong[7], Rui Su[7], Jianjun Chen[7], Shuan Rao[8], Ping Yi[4], Shuyang Yu[5], Fang Wang[1,2], and Jia Yu[1,2,9]

ABSTRACT

N^6-methyladenosine (m^{6}A) is the most prevalent internal RNA modification in mammals that regulates homeostasis and function of modified RNA transcripts. Here, we aimed to investigate the role of YTH m^{6}A RNA-binding protein 1 (YTHDF1), a key regulator of m^{6}A methylation in gastric cancer tumorigenesis. Multiple bioinformatic analyses of different human cancer databases identified key m^{6}A-associated genetic mutations that regulated gastric tumorigenesis. *YTHDF1* was mutated in about 7% of patients with gastric cancer, and high expression of YTHDF1 was associated with more aggressive tumor progression and poor overall survival. Inhibition of *YTHDF1* attenuated gastric cancer cell proliferation and tumorigenesis *in vitro* and *in vivo*. Mechanistically, YTHDF1 promoted the translation of a key Wnt receptor frizzled7 (*FZD7*) in an m^{6}A-dependent manner, and mutated *YTHDF1* enhanced expression of FZD7, leading to hyperactivation of the Wnt/β-catenin pathway and promotion of gastric carcinogenesis. Our results demonstrate the oncogenic role of *YTHDF1* and its m^{6}A-mediated regulation of Wnt/β-catenin signaling in gastric cancer, providing a novel approach of targeting such epigenetic regulators in this disease.

Significance: This study provides a rationale for controlling translation of key oncogenic drivers in cancer by manipulating epigenetic regulators, representing a novel and efficient strategy for anticancer treatment.

Graphical Abstract: http://cancerres.aacrjournals.org/content/canres/81/10/2651/F1.large.jpg.

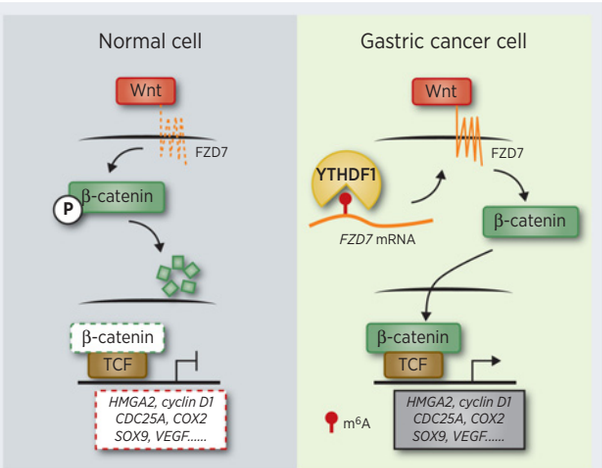

Increased YTHDF1 promotes gastric carcinogenesis by accelerating Wnt receptor gene FZD7 translation, leading to activation of the Wnt pathway in an m^{6}A-dependent manner.

Introduction

More than 100 distinct RNA modifications have been characterized in the last few decades, among which, the N^6-methyladenosine (m^{6}A) modification is the most abundant form in eukaryotic mRNA (1). RNA m^{6}A is highly conserved across plants (2), vertebrates (3), and also observed in viruses (4) as well as in single-cell organisms such as archaea (5), bacteria (6), and yeast (7). Recently, the reversible nature of m^{6}A modification was recognized because of the discovery of two RNA m^{6}A demethylases, α-ketoglutarate–dependent dioxygenase FTO and alkB homologue 5 (ALKBH5; refs. 8, 9). Since then, the mechanism underlying dynamic m^{6}A modification and its physiologic functions have attracted massive research interest. It is known that m^{6}A is incorporated into single-strand RNA molecules by a multicomponent methyltransferase complex containing METTL3, METTL14, and WTAP (10). Moreover, structured RNA can also be modified by another m^{6}A methyltransferase, METTL16 (11, 12). The transcriptome-wide RNA m^{6}A landscape was then preferentially distinguished by various m^{6}A readers (13). In the cytoplasm, the majority of YTH (YTHDF1-3 and YTHDC2) and IGF2BP (IGF2BP1-3) family proteins bind to m^{6}A-modified mRNAs and regulate their stability and translation (13–17). In addition, other proteins can bind m^{6}A-modified precursor RNAs in the nucleus and affect their processing (1, 18, 19).

Defects in m^{6}A-associated genes affect diverse biological processes. For example, depletion of METTL3 led to impaired embryonic stem

[1]State Key Laboratory of Medical Molecular Biology, Department of Biochemistry and Molecular Biology, Institute of Basic Medical Sciences, Chinese Academy of Medical Sciences, School of Basic Medicine, Peking Union Medical College, Beijing, China. [2]The Key Laboratory of RNA and Hematopoietic Regulation, Chinese Academy of Medical Sciences, Beijing, China. [3]Institute of Materia Medica, Chinese Academy of Medical Sciences and Peking Union Medical College, Beijing, China. [4]Department of Obstetrics and Gynecology, Affiliated Hospital of Chongqing Medical University, Chongqing, China. [5]State Key Laboratory of AgroBiotechnology, College of Biological Sciences, China Agricultural University, Beijing, China. [6]Department of Molecular Biology, Shanxi Cancer Hospital, Affiliated Cancer Hospital of Shanxi Medical University, Shanxi, China. [7]Department of Systems Biology and Gehr Family Center for Leukemia Research, The Beckman Research Institute of City of Hope, Monrovia, California. [8]Department of Thoracic Surgery, Nanfang Hospital, Southern Medical University, Guangzhou, China. [9]Medical Epigenetic Research Center, Chinese Academy of Medical Sciences, Beijing, China.

Note: Supplementary data for this article are available at Cancer Research Online (http://cancerres.aacrjournals.org/).

J. Pi and W. Wang are co-first authors of this article.

Corresponding Authors: Jia Yu, Institute of Basic Medical Sciences, Peking Union Medical College, No. 5 San Tiao Dongdan, Beijing 100005, China. Phone: 8610-6915-6423; Fax: 8610-6915-6423; E-mail: j-yu@ibms.pumc.edu.cn; and Fang Wang, wo_wfang@hotmail.com

Cancer Res 2021;81:2651–65

doi: 10.1158/0008-5472.CAN-20-0066

cell exit from self-renewal toward differentiation; inhibition of METTL14 resulted in conspicuous embryonic growth retardation (20); ablation of YTHDF2 in zebrafish embryos delayed maternal-to-zygotic transition in early embryonic development (21). Particularly, RNA m^6A-associated genes are emerging as crucial regulators contributing to tumor initiation and progression in various cancers (22–27), including METTL3 in lung cancer, METTL14 in liver cancer, FTO in leukemia, and ALKBH5 in breast cancer (22–27). However, how m^6A regulates carcinogenesis and how downstream pathways and mechanisms relay these signals are not fully understood.

Here, we aim to address these questions starting by searching for genomic mutations of canonical m^6A-associated writer, eraser, and reader genes in gastric cancer patients' samples. Consequently, *YTHDF1* emerged as the most frequently mutated m^6A reader gene in patients with gastric cancer. We then confirmed the overexpression of YTHDF1 in gastric tumor tissues compared with matched normal specimens, and higher YTHDF1 expression was indeed correlated with more malignant tumor phenotypes. Furthermore, reduced YTHDF1 expression could inhibit gastric tumorigenesis by altering the translation of a key Wnt receptor, frizzled 7 (FZD7), in an m^6A-dependent manner. Together, our results reveal YTHDF1 as an important factor promoting cancer progression and suggest that increased occupancy at m^6A sites is most likely an oncogenic mechanism underlying a large portion of gastric cancer cases. Finally, we identify m^6A methylation as a regulator of the Wnt/β-catenin signaling and gastric tumor cell growth.

Materials and Methods

Clinical specimens and cell lines

Samples of human gastric cancer tissues and paired adjacent nontumor gastric tissues from 113 patients were collected from Cancer Institute and Hospital, Chinese Academy of Medical Sciences (Beijing, China) and Shanxi Cancer Hospital (Taiyuan, ShanXi province, China; Supplementary Table S1). All the participants signed written informed consent form before recruitment. The study was conducted in accordance with the Declaration of Helsinki and approved by the Ethics Committee of Cancer Institute and Hospital, Chinese Academy of Medical Sciences and Shanxi Cancer Hospital. Gastric cancer tissues and paired adjacent noncancerous tissues (tissues microarray) were purchased from Outdo Biotech.

The cell lines MGC-803 and HGC-27 were obtained from ATCC in 2017. These cells were tested by short tandem repeat analysis, validated to be free of *Mycoplasma*, which were used within 6 months. In addition, the cells were cultured within 25 passages for all experiments. Gastric cancer cell lines, MGC-803 and HGC-27 were maintained in DMEM with 10% FBS (Hyclone) at 37°C in 5% CO_2 cell culture incubator.

Tissue microarray and IHC

Human gastric cancer tissue microarrays (TMA) containing 79 pairs of tumors and matched adjacent tissues were purchased from Shanghai Outdo Biotech. Co. Ltd (Supplementary Table S1). All samples were obtained with patient's informed content. After deparaffinization, rehydration, antigen retrieval, and blocking, the arrays were incubated overnight at 4°C with indicated antibodies. The slides were developed with DAB and counterstained with hematoxylin. The stained slides were observed under a microscope (Olympus 1 × 71) and images were acquired using software DP controller (ver. 3.1.1.267, Olympus). Stained tumor tissues and adjacent normal tissues were classified into four groups (0–3) according to the staining intensity of each tissue.

Cell proliferation, migration, and invasion assays

For the cell proliferation assays, shYTHDF1-1, shYTHDF1-2, and negative control transfected MGC-803 and HGC-27 cells were seeded in 96-well plates at 1,000 cells per well. Cell proliferation was evaluated by 10% CCK-8 (DOJINDO) diluted in normal culture media at 37°C diluted in normal culture media at 37°C until visual color conversion appears. Proliferation rates were determined at 0, 24, 48, 72, and 96 hours posttransfection, and quantification was done on a microtiter plate reader (Spectra Rainbow, Tecan) under manufacturer-recommended protocol.

For the cell migration and invasion transwell assays, shYTHDF1-1, shYTHDF1-2, and negative control transfected 60,000 MGC-803 or HGC-27 cells in 500 μL starvation media were plated on the top chambers of Transwell Clear Polyester Membrane Inserts (for the migration assay, Corning Costar) and BioCoat Matrigel Invasion Chambers (for the invasion assay, Corning Costar), while culture media with 20% FBS was applied on the bottom. After 48–72 hours, migrated or invaded cells were stained with crystal violet and counted under a ×20 microscope.

Animals

All experimental procedures involving animals were performed in accordance with the *Guide for the Care and Use of Laboratory Animals* (NIH publications nos. 80-23, revised 1996) and according to the institutional ethical guidelines of Peking Union Medical College (Beijing, China) for animal experiments.

In vivo tumorigenesis and metastasis formation assay

Stable short hairpin (shRNA)-expressing MGC-803 cells (3×10^6) were suspended in 0.1 mL PBS and injected into the flanks of BALB/c mice ($n = 8$ mice/group) at 5–6 weeks of age. For the flanks injected mice, tumor growth was examined every 3 days. After 5 weeks, mice were sacrificed by cervical dislocation, and weight of xenografts was tested.

BALB/c mice were randomly divided into three groups ($n = 4$ mice/group). A total of 3×10^6 stable shRNA-expressing MGC-803 cells were resuspended in 0.1 mL PBS and injected into the abdominal cavity. After 4 weeks, mice were sacrificed by cervical dislocation, abdominal cavities were opened, and the numbers of implantation metastasis were counted.

For the pulmonary metastasis model, NOD/SCID mice were randomly divided into three groups ($n = 4$ mice/group). A total of 1×10^5 stable shRNA-expressing MGC-803 cells were resuspended in 0.1 mL PBS and injected into the lateral tail vein. After 7 weeks, mice were sacrificed by cervical dislocation, and lungs were extracted and fixed 4% paraformaldehyde in PBS. Paraffin embedding, sectioning, and staining with hematoxylin and eosin were performed. Visible lung metastases were measured and counted using a microscope.

Patient-derived xenograft

The patient-derived xenograft (PDX) samples were obtained in Beijing IDMO company (Supplementary Table S1). The 0.5 cm^3 xenograft tumor tissues were implanted into the subcutaneous pocket on the SCID mice for amplification of the PDX samples. Two weeks after the tumor transplantation, the mice were randomized into different groups: siControl; siYTHDF1 ($n = 4$ mice/group), and treated with different siRNA formulations (2 nmol siRNA per mouse equivalent) via subcutaneous injection every 2 days for eight injections. On day 25, the mice were killed, tumor xenografts and associated mesenteries were excised, weighted, and imaged.

RNA Isolation and qPCR analysis

Total RNA was extracted from cells and tissues using TRIzol (Invitrogen) according to the manufacturer's instruction. qPCR primers used are listed in Supplementary Table S2. See Supplementary Materials and Methods for additional details.

Plasmids

YTHDF1-WT, YTHDF1-MUT (K395A, Y397A), FZD7 Peak1 mutation, FZD7 Peak2 mutation, and FZD7 Peak1&Peak2 mutation expression plasmids were cloned into pcDNA3.1 vector (IDOBIO). See Supplementary Table S3 for additional details.

Lentiviral transfection

All lentiviral vectors for YTHDF1 knockdown were designed into pLKO.1 vector (kindly provided by Dr. Jianjun Chen, the Beckman Research Institute of City of Hope, Duarte, CA). The target sequence of the two shRNA (shYTHDF1) was 5′-GATACAGTTCATGACAATGA-3′ and 5′-GAAACGTCCAGCCTAATTCT-3′. The lentiviral vectors were cotransfected with packaging vectors psPAX2 (Addgene) and pMD2G (Addgene) into 293T cells for lentivirus production. See Supplementary Materials and Methods for additional details.

Immunofluorescence assay

Immunofluorescence (IF) assay was performed as described previously (28). See Supplementary Materials and Methods for additional details.

IHC, hematoxylin and eosin staining, and light microscopy

IF assay was performed as described previously (29). See Supplementary Materials and Methods for additional details.

Polysome profiling

MGC-803 cells were infected with lentiviral shRNA targeting YTHDF1 and treated with cycloheximide at 100 μg per mL for 10 minutes before collection. Cells were pelleted, lysed on ice, and centrifuged. The supernatant was collected and loaded onto a 10/50% w/v sucrose gradient prepared in a lysis buffer without Triton X-100. The gradients were centrifuged at 4°C for 4 hour at 27,500 rpm (Beckman, rotor SW28). The sample was then fractioned and analyzed by Gradient Station (BioCamp) equipped with an ECONO UV monitor (Bio-Rad) and fraction collector (FC203B, Gilson). The fractions were categorized and used for RNA by TRIzol reagent for RT-PCR.

Western blot analysis

Western blot analysis was performed as described previously (30). The details of the antibodies are in Supplementary Materials and Methods.

RNA-seq

Total RNA was isolated from YTHDF1 control or knockdown MGC-803 cells using TRIzol reagent. Poly(A) RNA was subsequently purified from 50 to 100 ng total RNA using PolyTtract mRNA Isolation System. NEBNext Ultra RNA Library Prep Kit for Illumina (New England BioLabs) was used for library preparation. Each group was sequenced in duplicate.

RNA Immunoprecipitation assay

MGC-803 cells were seeded in a 10-cm dish at 70%–80% confluence. A total of 5 μg of YTHDF1 (17479-1-AP, Proteintech) antibody and a corresponding control rabbit IgG (NI01, Millipore) were conjugated to protein A/G magnetic beads (Thermo Fisher Scientific) by incubation for 4 hours at 4°C, followed by washing three times and incubation with lysate of MGC-803 cells in RNA immunoprecipitation (RIP) buffer [150 mmol/L KCl, 25 mmol/L Tris (pH 7.4), 5 mmol/L EDTA, 0.5 mmol/L DTT, 0.5% NP40, 1 × protease inhibitor] at 4°C overnight. After washing with RIP buffer for three times, beads were resuspended in 80 μL PBS, followed by DNA digestion at 37°C for 15 minutes and incubation with 50 μg of proteinase K (Thermo Fisher Scientific) at 37°C for 15 minutes. Input and coimmunoprecipitation RNAs were recovered by TRIzol, extraction and analyzed by qPCR or RNA sequencing (RNA-seq).

m^{6}A-RNA IP Assay

Total RNAs were extracted from MGC-803 cells and purifying with PolyTtract mRNA Isolation System (Promega). Chemically fragmented RNA (100 nucleotides) was incubated with m^{6}A antibody for IP according to the standard protocol of the Magna methylated RIP (MeRIP) m^{6}A Kit (Merck Millipore). Enrichment of m^{6}A containing mRNA was then analyzed either through qPCR or by high-throughput sequencing. For high-throughput sequencing, purified RNA fragments from m^{6}A-MeRIP were used for library construction with the NEBNext Ultra RNA library Prep Kit for Illumina (New England BioLabs) and were sequenced with Illumina HiSeq X-10. Library preparation and high-throughput sequencing were performed by Novogene.

CLIP Assay

CLIP was performed following previously reported protocol (31). In brief, whole-cell extract prepared from 1.5×10^7 YTHDF1 overexpressed MGC-803 cells was used for IP reaction and prepared into eCLIP-qPCR. The method used UV cross-linking of intact cells to covalently link RNA to cellular RNA-binding proteins. Whole-cell extracts were prepared, followed by RNase I digestion to fragment the RNA prior to IP of target proteins and associated bound RNAs. We performed eCLIP using whole-cell extract from MGC-803 cells and Flag antibody (M185-3L, MBL). The RNA-binding protein complexes were isolated from polyacrylamide gels based on the expected molecular weight of YTHDF1 a 70-kDa region. The bound protein was degraded, and RNA was isolated and further processed into eCLIP-qPCR.

Sequencing data analysis

For RIP-seq data: samples were sequenced by Illumina HiSeq X-ten with pair-end 150-base pair (bp) read length. The RIP-seq reads were mapped to human genome version hg19 by Tophat2 version 2.1.1 with default settings (32). The RIP targets were defined as genes with $\log_2$ (IP/input)>0 and $P < 0.05$.

For RNA-seq data: all RNA-seq samples were sequenced by Illumina HiSeq X-ten with pair-end 150-bp read length. All reads were mapped to human genome version hg19 by Tophat2 version 2.1.1 with default settings (32). Read counts were calculated using HTSeq (32). Differential gene expression was calculated by DESeq2 ($\log_2$ KD/NC>1, $P < 0.05$).

For m^{6}A-seq: samples were sequenced by Illumina HiSeq X-ten with pair-end 150-bp read length. All reads were mapped to human genome version hg19 by Tophat2 version 2.1.1 with default settings (32). The m^{6}A level changes for IP/input were calculated by using MACS (33; $Q < 0.05$).

Pathway enrichment analysis

The web-based tool (https://david.ncifcrf.gov/) was used for enrichment analysis of differentially expressed genes (DEG) screened by RNA-seq (34, 35). The web-based tool (http://metascape.org/gp/index.html#/main/step1) was used for enrichment analysis of YTHDF1-binding genes and direct targets of YTHDF1.

Data availability

The raw sequence data reported in this article have been deposited in the Genome Sequence Archive (36) in BIG Data Center (37), Beijing Institute of Genomics (BIG), Chinese Academy of Sciences, under accession numbers CRA001261 that are publicly accessible at https://bigd.big.ac.cn/gsa. The human cancer data were derived from The Cancer Genome Atlas (TCGA) Research Network (http://cancergenome.nih.gov/). The dataset [(stomach adenocarcinoma (38), $n = 100$; stomach adenocarcinoma (39), $n = 478$; stomach adenocarcinoma (40), $n = 30$; stomach adenocarcinoma (41), $n = 22$] derived from this resource that supports the findings of this study is available in the cBioPortal for Cancer Genomics (http://www.cbioportal.org/).

Statistical analysis

Each experiment was repeated at least three times. The Student *t* test (two-tailed unpaired *t* test) was performed for two-group data and three-group data were analyzed using one-way ANOVA with Newman–Keuls *post hoc* test. The test was used to examine the relationships between YTHDF1 expression and clinicopathologic characteristics. Kaplan–Meier analysis and log-rank test were used to evaluate the differences in patient survival. The Spearman rank correlation test was conducted for statistical correlations. All data were analyzed using GraphPad Prism 5.0 software (GraphPad Software, Inc.) or SPSS 16.0 software (SPSS Inc.) and presented as means ± SD.

Ethics

The use of clinical samples in this study was approved by the institutional review board of Institute of Basic Medicine, Chinese Academy of Medical Science. All experimental procedures involving animals were performed in accordance with The Guide for the Care and Use of Laboratory Animals (NIH publications nos. 80-23, revised 1996) and according to the institutional ethical guidelines of Peking Union Medical College (Beijing, China) for animal experiments.

Results

YTHDF1 Gene amplifications in gastric cancer

To interrogate the genetic alterations of m^6A-associated genes involved in gastric cancer development, cBioPortal (cBio Cancer Genomics Portal) datasets including 630 primary gastric adenocarcinomas were analyzed. Notably, the YTH family readers (expect for *YTHDF2*) showed relatively higher mutation rates compared with writers and erasers. Of note, *YTHDF1* was the most prevalent mutated gene that occurred in about 7% of all patients with gastric cancer. By evaluating the distribution of *YTHDF1* mutations, we observed 65% of all mutations were gene amplifications, which usually resulted in the overexpression of gene products (**Fig. 1A**; Supplementary Fig. S1A). We then explored TCGA datasets including 24 different cancer types and found that YTHDF1 expression was indeed significantly higher in patients with gastric cancer than normal tissues (**Fig. 1B**). In addition, although *YTHDF1* mutations were not common in diverse cancers (Supplementary Table S4), the upregulation of YTHDF1 was observed in most tumors, suggesting a general oncogenic role for *YTHDF1* in cancer development (**Fig. 1B**). Particularly, higher YTHDF1 expression was correlated with gastric cancer progression (**Fig. 1C**) and poor overall survival (**Fig. 1D**).

We next verified these *in silico* findings in 113 pairs of in-house gastric cancer tissues and matched noncancerous tissues by qPCR. Indeed, *YTHDF1* mRNA was significantly increased in gastric cancer tumors ($P = 0.0005$; **Fig. 1E**; Supplementary Fig. S1B). IHC analysis of both normal gastric tissues and gastric cancer specimens confirmed the upregulation of YTHDF1 protein in tumor tissues (**Fig. 1F**). Furthermore, the aberrantly high expression of YTHDF1 in patients with gastric cancer was significantly correlated with more severe clinical pathologic characteristics such as perineural invasion, aggressive tumor stage (stage III/IV vs. I/II), and venous invasion (**Fig. 1G**; Supplementary Table S5). Kaplan–Meier survival analysis also showed that patients with gastric cancer with high YTHDF1 expression exhibited a worse 4-year overall survival [log-rank (Mantel–Cox) $P = 0.0075$; **Fig. 1H**; Supplementary Table S6]. These data collectively suggest a potential oncogenic role of YTHDF1 in gastric tumorigenesis.

YTHDF1 deficiency inhibits gastric cancer progression and metastasis

We measured the protein expression level of YTHDF1 in various gastric cancer cell lines, which were much higher than the normal gastric gland cell GES-1 (Supplementary Fig. S2A). To further explore YTHDF1's function in gastric cancer, we applied different systems, including gastric cancer cell lines, cell line–derived xenograft (CDX), and PDX models (**Fig. 2A**). First, we investigated the effects of knocking down YTHDF1 by generating two stable shRNA-expressing human gastric cancer cell lines, MGC-803 and HGC-27, which displayed relatively higher YTHDF1 expression among all tested gastric cancer cell lines (Supplementary Fig. S2B). YTHDF1 knockdown indeed decreased cell proliferation in gastric cancer cells (**Fig. 2B**). Furthermore, YTHDF1 deficiency in both MGC-803 and HGC-27 cells impaired their migration and invasion abilities (**Fig. 2C**; Supplementary Fig. S2C). We next examined whether inhibition of YTHDF1 could affect gastric cancer tumorigenesis *in vivo* by subcutaneously injecting YTHDF1-deficent MGC-803 cells into immunocompromised nude mice. Consistently, reduced YTHDF1 levels resulted in delayed tumor progression of MGC-803–engrafted tumors (Supplementary Fig. S2D and S2E), as the weight and volume in YTHDF1-deficient tumors were significantly decreased compared with YTHDF1-competent tumors (**Fig. 2D**). Accordingly, the proliferation marker Ki-67 was downregulated and the apoptotic marker cleaved caspase-3 was upregulated in YTHDF1-deficient tumors (**Fig. 2E**).

We then explored whether YTHDF1 could contribute to gastric cancer metastasis *in vivo* with two metastasis models. Tail vein injection of YTHDF1-competent MGC-803 cells resulted in pulmonary metastases, whereas knocking down of YTHDF1 almost completely abolished metastatic node formation (**Fig. 2F**; Supplementary Fig. S2F). In the peritoneal metastatic xenograft model, injection of YTHDF1-deficent MGC-803 cells also significantly decreased secondary tumor formation in the abdominal cavity (Supplementary Fig. S2G). All these results confirmed the oncogenic role of YTHDF1 in gastric carcinogenesis by regulating cell proliferation and metastasis.

To further confirm the conclusions derived from the *in vivo* and *ex vivo* studies, we established the PDX model, our results showed that knocking down YTHDF1 suppressed tumor growth and weights (**Fig. 2G–I**; Supplementary Fig. 2H). Moreover, Ki-67 expression in siYTHDF1-treated tumors was significantly decreased while cleaved caspase-3 in siYTHDF1 tumors was significantly increased as

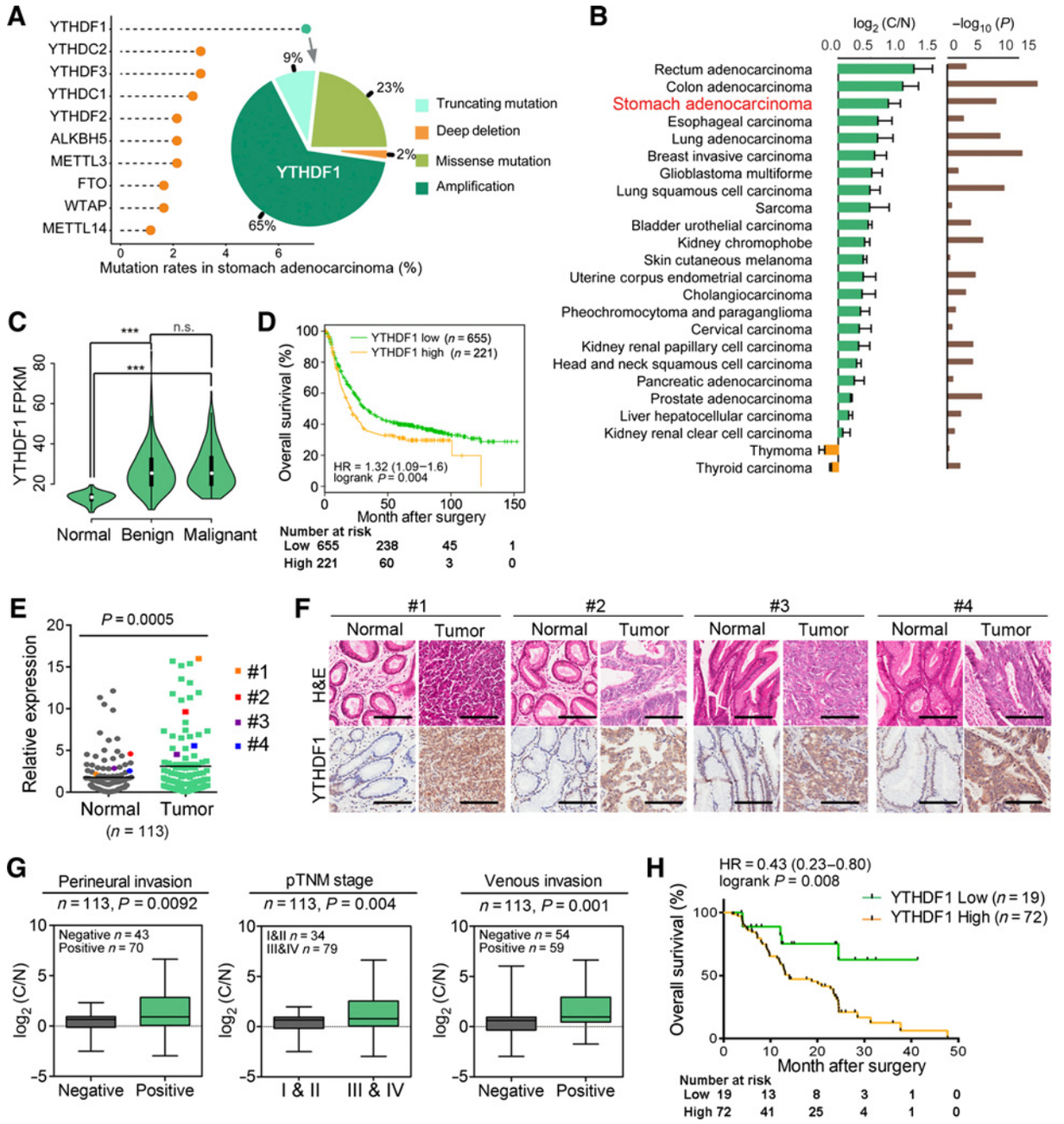

Figure 1.

Overexpression of YTHDF1 in gastric cancer. **A,** Gene mutation rates of the top 10 m^{6}A-associated genes in gastric cancer according to cBioPortal datasets ($n = 630$). Distributions of different mutation subtypes in *YTHDF1* gene are shown as a pie chart (right). **B,** Relative expression alternations of YTHDF1 in cancer tissues compared with the matched normal tissues according to TCGA datasets including 24 types of cancer. **C,** Violin plot of YTHDF1 expression in normal, benign, or malignant gastric tissues (normal, $n = 32$; benign, $n = 164$; malignant, $n = 188$). **D,** Overall survival rates for patients with high YTHDF1 expression ($n = 215$) versus low YTHDF1 expression ($n = 58$) generating from public gastric cancer cohorts (kmplot.com), profiled with GSE29272. **E,** Relative YTHDF1 expression in 113 pairs of gastric tumors and adjacent normal tissue ($n = 113$). **F,** Representative IHC images of YTHDF1 in four gastric tumor tissues and corresponding normal tissues. Scale bar, 100 μm. **G,** Correlations of YTHDF1 expression with perineural invasion (left), TNM stages (middle), and venous invasion (right) of patients with gastric cancer ($n = 113$). **H,** Kaplan–Meier survival analysis showed the correlation of YTHDF1 expression (low, $n = 19$; high, $n = 72$) and overall survival rate of patients with gastric cancer (log-rank with Mantel–Cox test). ***, $P < 0.001$ (one-way ANOVA); n.s., nonsignificant. All data are shown as means ± SD.

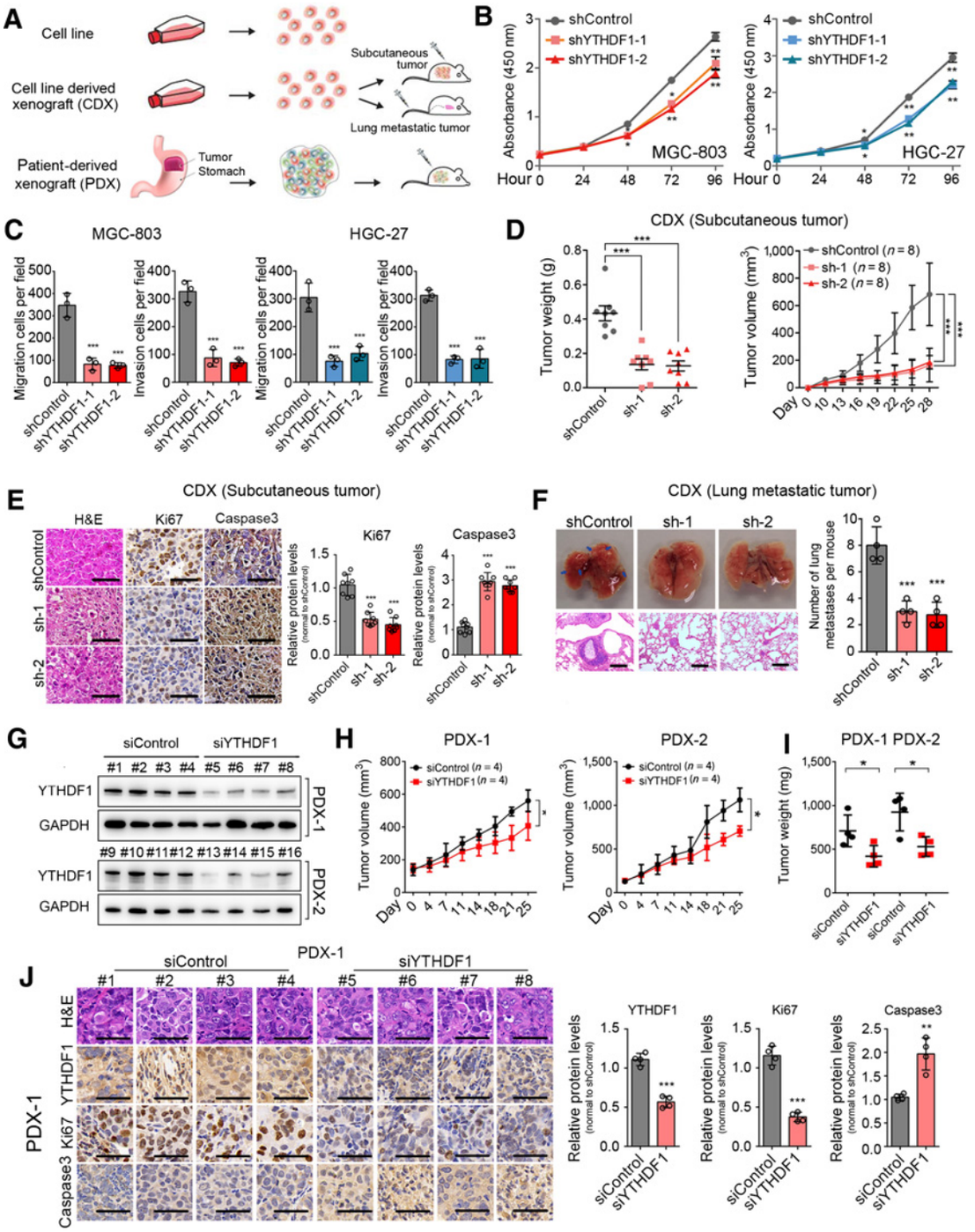

Figure 2.

YTHDF1 is important for tumor cell proliferation, migration, and invasion. **A,** Schematic diagram strategies for dissecting YTHDF1's function *in vivo* and *in vitro*. **B,** Analysis of cell proliferation in YTHDF1 knockdown MGC-803 and HGC-27 cells ($n = 3$). **C,** Transwell migration and invasion assays of MGC-803 and HGC-27 cells stably expressing shRNAs targeting YTHDF1 or scramble control ($n = 3$). **D,** Quantification of tumor weight (left) and tumor growth (right) using CDX model; also see online Supplementary Fig. S2D for tumor volumes ($n = 8$). **E,** Representative IHC images and quantification of Ki-67 and caspase-3 positive staining in CDX model ($n = 8$). Scale bar, 50 μm. **F,** Representative images and histology images of pulmonary metastases in mice lung metastasis model ($n = 4$). Blue arrows, metastatic nodules. Scale bar, 100 μm. **G** and **H,** The tumor growth analysis of PDX models with siControl or siYTHDF1 treatment. **I,** Comparison of tumor weight of PDX models with siControl or siYTHDF1 treatment. **J,** Representative histology images and IHC results of YTHDF1, Ki-67, and caspase-3 in PDX models. Scale bar, 50 μm. The quantification of IHC is shown on the right ($n = 4$). *, $P < 0.05$; **, $P < 0.01$; ***, $P < 0.001$ [Student *t* tests (**H** and **I**) or one-way ANOVA (**B**, **C**, **D**, **E**, and **F**)]. All data are shown as means ± SD.

compared with the siControl tumors (**Fig. 2J**; Supplementary Fig. S2I). These data also revealed YTHDF1 plays an important role in gastric cancer tumorigenesis.

Identification of YTHDF1-regulated transcripts by RNA-seq, RIP-seq, and MeRIP-seq

To comprehensively understand the effect of YTHDF1 deficiency on gastric cancer development, we performed RNA-seq analysis with YTHDF1 knockdown and control MGC-803 cells. RNA profiling revealed different subsets of transcripts that were dysregulated upon YTHDF1 inhibition (**Fig. 3A**; Supplementary Table S7). Gene ontology (GO) analysis indicated that those downregulated genes were enriched for angiogenesis, cell migration, adhesion, and cell growth; whereas genes mapped to negatively regulated tumor progression were upregulated (**Fig. 3B**), supporting the previous finding that YTHDF1 is an oncogenic factor in gastric cancer. We next screened for YTHDF1-binding genes by using RIP-seq within MGC-803 cells. When a gene specifically binds to Input but not IgG, then we defined it as a gene that specifically binds to YTHDF1. With this standard, we obtained 9,082 candidate genes (Supplementary Table S7). We analyzed those top 3,000 most significant changed genes for functional enrichment, which indicated that they were highly involved in cancer-related pathways (**Fig. 3C**). However, the cumulative distribution analysis suggested that there was no significant difference between the YTHDF1-bound genes and the YTHDF1 unbound genes at transcription level (**Fig. 3D**). This is consistent with the previous finding that YTHDF1 mainly regulates the gene translation. (14)

Because YTHDF1 is a well-known m^6A-specific reader protein (14), we then intended to identify potential transcripts with m^6A modification that were regulated by YTHDF1 using MeRIP-seq within MGC-803 cells. m^6A modification was detected in 2,365 transcripts, which predominantly occurred with mRNAs (98%; **Fig. 3E**; Supplementary Table S7), preferentially clustered in the exons (58%; **Fig. 3E**). In line with other N^6-methyladenosine–sequencing results, the m^6A peaks were enriched in 3′UTR regions (**Fig. 3F**) and exclusively detected with the canonical GGAC motifs (**Fig. 3G**).

To search the direct targets of YTHDF1, we then overlapped the transcripts identified by YTHDF1-specific RIP-seq and MeRIP-seq (**Fig. 3H**; Supplementary Table S7). Enrichment analysis with these transcripts revealed the Wnt and Hippo signaling pathways were dramatically affected (**Fig. 3H**; Supplementary Table S7), both pathways had been shown to be critical for tumor progression and were frequently mutated in various cancers, we therefore hypothesized that YTHDF1 inhibition suppressed tumor growth via the Hippo or Wnt pathways (**Fig. 3I**; Supplementary Table S7).

FZD7 is a bona-fide m6A modification target of YTHDF1

In total 13 transcripts (**Fig. 3I**, highlighted in orange color) allocated to Hippo or Wnt pathways exhibited high m^6A peaks as determined by MeRIP-seq. To verify the bona-fide YTHDF1 targets in gastric cancer, we employed a multiple steps screening strategy (**Fig. 4A**). First, we determined YTHDF1 interacted transcripts using RIP combined with qPCR validation (**Fig. 4B**; Supplementary Fig. S3A). Transcripts including *FZD1, FZD7, CTBP2, MAPK9*, and *MAP3K7* attribute to the Wnt pathway, as well as *TP53BP1, PARD3, SMAD2*, and *SMAD3* belong to Hippo pathway were effectively immunoprecipitated by YTHDF1 antibody specifically (**Fig. 4C**; Supplementary Fig. S3A). Given the notion that YTHDF1 could regulate target genes' expression at translational level, we then detected these candidates' expression in YTHDF1-deficient cells. Interestingly, YTHDF1 knockdown only markedly reduced the protein levels of FZD7, MAPK9, SMAD2, SMAD3, and PARD3 (**Fig. 4D**) although their mRNA was not affected (Supplementary Fig. S3B).

Furthermore, the m^6A immunoprecipitation (m^6A-IP) and YTHDF1 enhanced cross-linking immunoprecipitation (eCLIP) followed by qPCR (Supplementary Fig. S3C) confirmed both the presence of m^6A modification and the occupancy by YTHDF1 at *FZD7, MAPK9, SMAD2 SMAD3*, and *PARD3* mRNAs (**Fig. 4E** and **F**). Next, we performed polysome profiling, a method that allows monitoring translation activity of specific mRNAs to verify whether YTHDF1 could regulate the candidates' translation in gastric cancer cells. As expected, YTHDF1 knockdown showed general translational suppression as the polysome association was gradually decreased in YTHDF1-deficient MGC-803 cells (**Fig. 4G**). Of note, the translation efficiency of *FZD7* was the most significantly downregulated while other genes showed mild translation suppression (**Fig. 4G**). Taken together, these results collectively suggested that FZD7 is the bona-fide direct target of YTHDF1 in gastric cancer.

YTHDF1 regulates FZD7 expression in an m6A-dependent manner

As a well-characterized oncogene, *FZD7* is known to be activated in patients with gastric cancer to promote epithelial-to-mesenchymal transition (42, 43). To validate and expand our previous findings, another gastric cancer cell line HGC-27 in addition to MGC-803 was employed for the gene-specific m^6A-qPCR as well as YTHDF1 RIP-qPCR analysis, respectively. Indeed, two m^6A peaks among *FZD7* mRNA were observed and the association with YTHDF1 was confirmed in both MGC-803 and HGC-27 cells (**Fig. 5A** and **B**).

We then questioned whether the YTHDF1-regulated *FZD7* translation was m^6A modification dependent. To address this, a Flag-tagged mutant YTHDF1 construct (YTHDF1-MUT) with two key amino acids mutations (K395A, Y397A) to abolish its m^6A-binding pockets (44) was transfected into both MGC-803 and HGC-27 cells (**Fig. 5C**; Supplementary Fig. S4). After introducing these mutations, the upregulation of FZD7 expression observed in wild-type YTHDF1 (YTHDF1-WT) transfected gastric cancer cells was eliminated in YTHDF1-MUT due to the m^6A reader activity deficiency (**Fig. 5D**), but the mRNA levels of FZD7 were comparable between YTHDF1-WT and YTHDF1-MUT in both cell lines (**Fig. 5E**). Accordingly, RIP-qPCR analysis revealed that the interaction between *FZD7* mRNA and mutant YTHDF1 was obviously impaired (**Fig. 5F**).

To further explore the involvement of m^6A modifications in *FZD7* mRNA, we constructed three types of *FZD7* mutants with mutation either in the first (FZD7-Peak1 Mut) or second (FZD7-Peak2 Mut) m^6A peak, as well as the double mutants (FZD7-Peak1&2 Mut; **Fig. 5G**). Interestingly, as compared with wild-type FZD7 (FZD7-WT), mutations within the second m^6A peak and the double m^6A peaks mutant (FZD7-Peak2 Mut and FZD7-Peak1&2 Mut) had no response to wild-type YTHDF1 overexpression (**Fig. 5H**, panels 7 and 8), suggesting the second m^6A peak in FZD7 was the key site for YTHDF1's regulation. Again, loss of m^6A-binding ability entirely abrogated the effect of YTHDF1 in promoting *FZD7* mRNA translation (**Fig. 5H**, panels 9–12). These results indicated that the translational control of *FZD7* mediated by YTHDF1 was dependent on m^6A modification.

YTHDF1 regulates Wnt/β-catenin pathway through FZD7

Upon binding of Wnt ligands to frizzled receptors, β-catenin is stabilized and translocating into the nucleus (the activated form), where it interacts with other coactivators to activate downstream gene

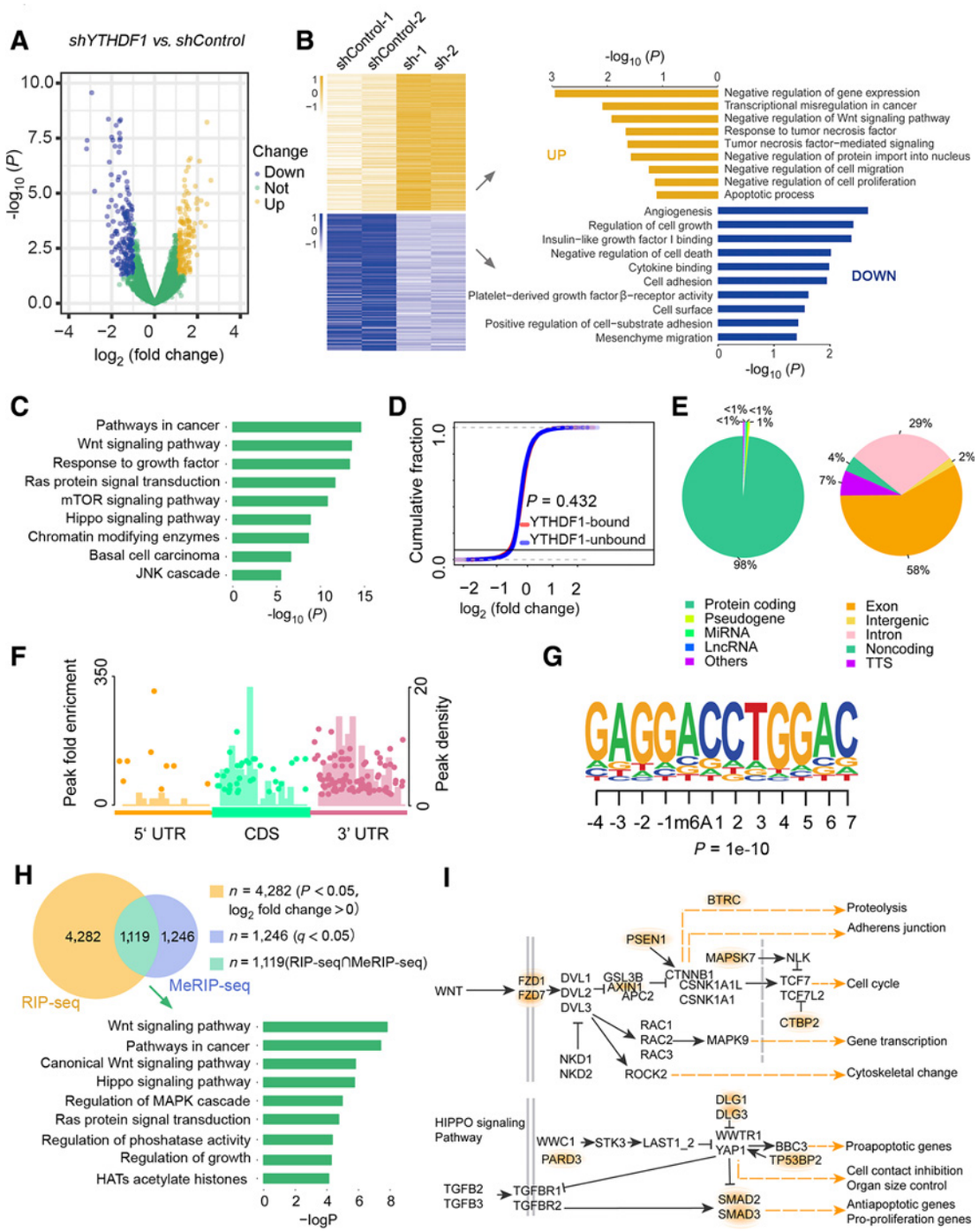

Figure 3.

Transcriptome-wide identification of YTHDF1 targets in gastric cancer. **A,** Volcano plot of DEGs in MGC-803 cells stably expressing shRNAs targeting YTHDF1 or scramble control. Green, unchanged genes when compared between YTHDF1 knockdown and control group ($|\log_2$ fold change $< 1|$ or $P > 0.05$). Yellow, upregulated genes ($\log_2$ fold change > 1 and $P < 0.05$) in YTHDF1 knockdown group. Blue, downregulated genes ($\log_2$ fold change < -1 and $P < 0.05$). **B,** DEGs identified by RNA-seq are presented in heatmap and GO enrichment analysis of DEGs. **C,** Functional enrichment of 5,401 genes detected by RIP-seq. **D,** Cumulative distribution map of YTHDF1 bound and unbound genes expression. **E,** The distribution of m^6A peaks in different RNA subgroups. **F,** The distribution of m^6A-modified locations in transcripts as identified by m^6A-seq in gastric cancer cells. **G,** Sequence logo representing the MEME-deduced consensus motifs identified by m^6A-seq. **H,** The overlapping of m^6A-modified mRNAs detected by MeRIP-seq and recognized YTHDF1 bind transcripts identified in RIP-seq (top). The functional enrichment of 1,119 overlapped genes detected by RIP-seq and MeRIP-seq (bottom). **I,** Kyoto Encyclopedia of Genes and Genomes annotated diagram of the Wnt and Hippo signaling pathways with highlighted genes affected by m^6A modification labeled in orange.

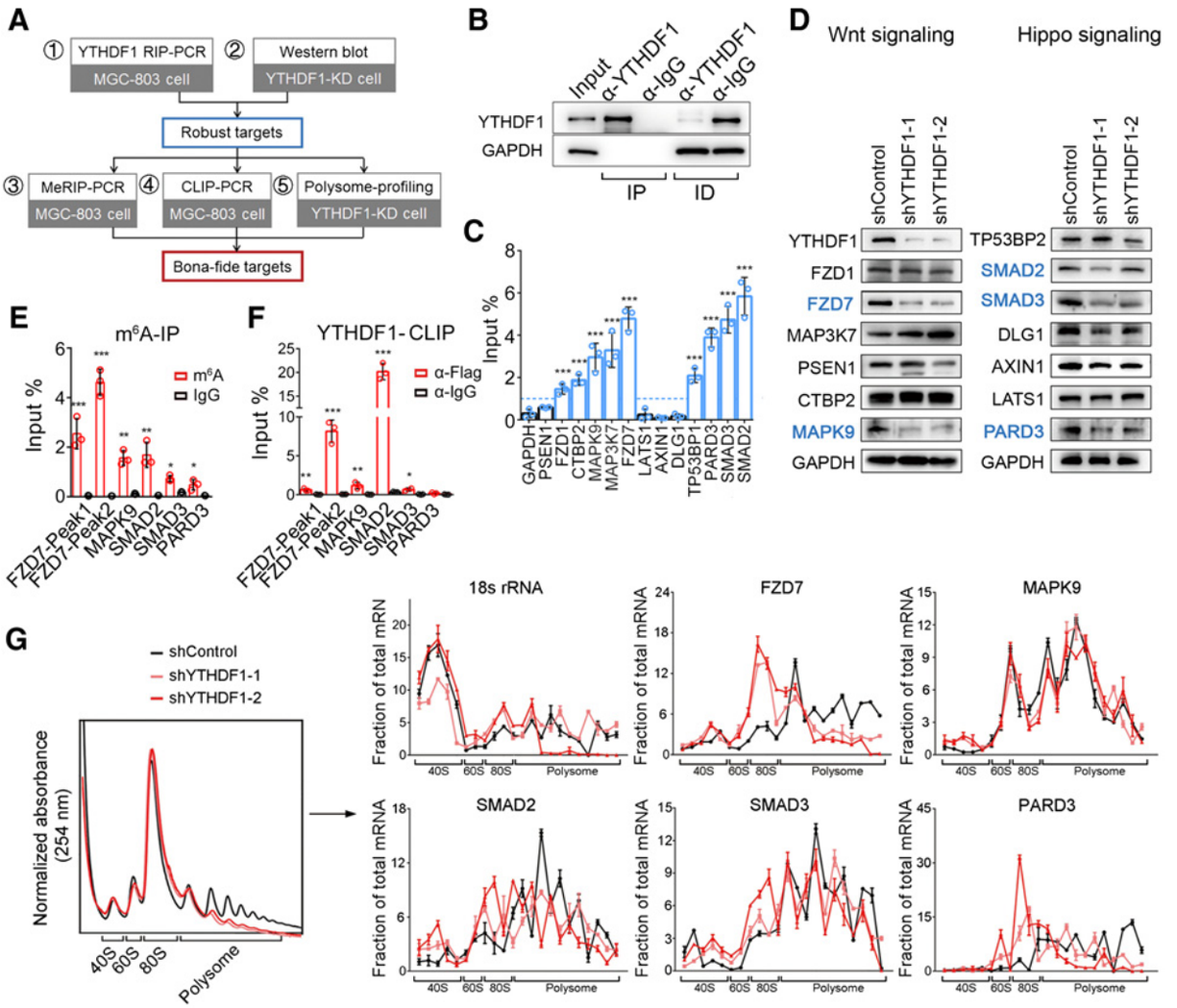

Figure 4.

Screening of YTHDF1 targets in gastric cancer cells. **A,** Schematic diagram strategies for screening of YTHDF1 targets. **B,** Western blot detection of precipitated proteins with endogenous YTHDF1 RIP analysis. IP, the precipitated fractions; ID, the depleted supernatants. **C,** Gene-specific qPCR analysis of the coprecipitated RNAs by YTHDF1 antibodies in RIP analysis ($n = 3$). **D,** Western blot analysis of YTHDF1-targeted candidates in YTHDF1 knockdown MGC-803 cells. Blue, proteins significantly decreased. **E,** Gene-specific m^{6}A qPCR validation of m^{6}A levels in MGC-803 cells ($n = 3$). **F,** Gene-specific qPCR analysis of the coprecipitated RNAs by Flag antibodies in flag-tagged YTHDF1 CLIP analysis ($n = 3$). **G,** Left, polysome-profiling assay in YTHDF1 knockdown and control MGC-803 cells. Right, qPCR analysis of FZD7, MAPK9, SMAD2, SMAD3, and PARD3 transcripts in different polysome fractions. The 18s rRNA was used as a quality control. *, $P < 0.05$; **, $P < 0.01$, ***, $P < 0.001$ (Student t tests). All data are shown as means ± SD.

transcription (**Fig. 6A**). Because FZD7 can activate the canonical Wnt signaling in gastric cancer cells (42) and YTHDF1 is a positive regulator for FZD7's expression, we hypothesized that YTHDF1 could directly regulate the Wnt pathway. To test this hypothesis, total and activated β-catenin was examined, respectively. As expected, when FZD7 expression was inhibited after knocking down YTHDF1, we also observed decreased expression of total and activated β-catenin in both MGC-803 and HGC-27 cells (**Fig. 6B**). Furthermore, only wild-type YTHDF1, but not the mutant form, increased FZD7 and activated β-catenin expression in gastric cancer cells (**Fig. 6B**), indicating that YTHDF1 activated β-catenin in an m^{6}A-dependent manner. Using IF staining, we observed that gastric cancer cells overexpressing the wild-type YTHDF1 but not the mutant form displayed a more intensive and accumulated β-catenin staining (**Fig. 6C**). In contrast, the YTHDF1 knockdown cells displayed less accumulation of β-catenin compared with the control cells (**Fig. 6C**). Consistently, other six known downstream players of the Wnt/β-catenin pathway, including high mobility group AT-hook 2 (HMGA2), cyclin D1, cell division cycle 25A (CDC25A), cytochrome c oxidase subunit II (COX2), SRY-box 9 (SOX9), and VEGF A (VEGFA) were regulated in a similar way as β-catenin at both transcriptional and translational levels, that is upregulated in wild-type but not mutant YTHDF1-overexpressing cells, whereas downregulated in YTHDF1 knockdown cells (**Fig. 6D** and **E**). In addition, there was also a strong correlation between YTHDF1 level and the expression of these β-catenin targets in a gastric cancer dataset from Gene Expression Omnibus database

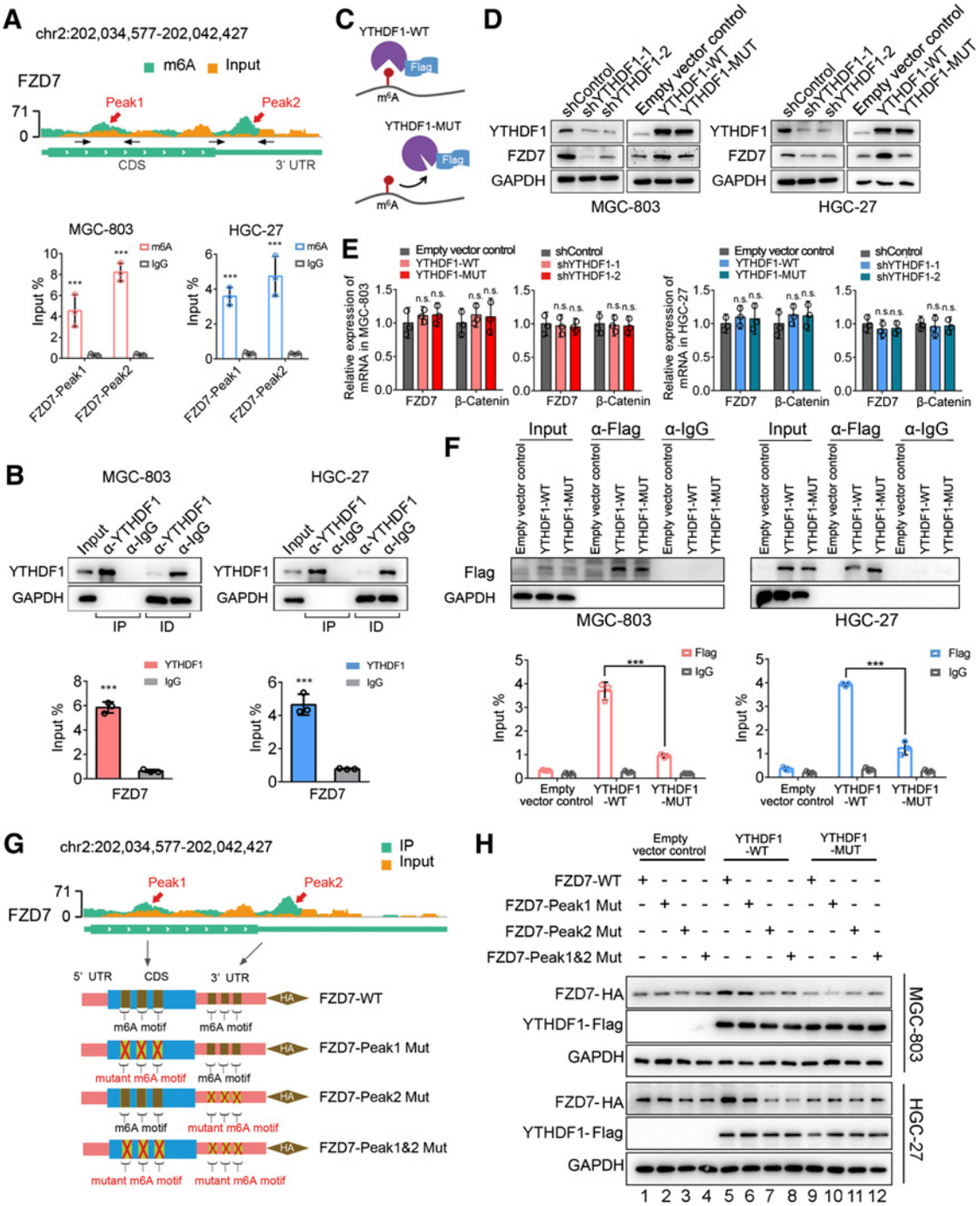

Figure 5.

YTHDF1 regulates FZD7 translation in an m^{6}A-dependent manner. **A,** Gene-specific m^{6}A qPCR validation of m^{6}A levels on *FZD7* mRNA in MGC-803 and HGC-27 cells ($n = 3$). **B,** Western blot detection of precipitated proteins in endogenous YTHDF1 RIP analysis. IP, the precipitated fractions; ID, the depleted supernatants (top). FZD7-specific qPCR analysis of the coprecipitated RNAs by YTHDF1 antibodies in RIP analysis ($n = 3$; bottom). **C,** Schematic description of wild-type (YTHDF1-WT) and mutant (YTHDF1-MUT) YTHDF1 constructs. **D,** Protein level of FZD7 in YTHDF1 knockdown, overexpressed, or mutant-overexpressed MGC-803 and HGC-27 cells. **E,** RNA level of FZD7 in YTHDF1 knockdown, overexpressed, or mutant-overexpressed MGC-803 and HGC-27 cells ($n = 3$). **F,** Western blot detection of precipitated proteins in Flag-tagged YTHDF1 RIP analysis. IP, the precipitated fractions; ID, the depleted supernatants (top). FZD7-specific qPCR analysis of the coprecipitated RNAs by Flag antibodies in RIP analysis ($n = 3$; bottom). **G,** Schematic illustration of different HA-tagged FZD7 constructs, comprising wild-type (FZD7-WT), and mutations of the m^{6}A motifs in m^{6}A peak1 (FZD7-Peak1 Mut), peak2 (FZD7-Peak2 Mut), or double mutants (FZD7-Peak1&2 Mut). **H,** Protein level of HA-tagged FZD7 in MGC-803 or HGC-27 cells cotransfected with empty vector (control), wild-type or mutant Flag-tagged YTHDF1, and wild-type or mutant HA-tagged FZD7 as described in **G**. *, $P < 0.05$; **, $P < 0.01$; ***, $P < 0.001$; n.s., nonsignificant (Student *t* tests). All data are shown as means ± SD.

(GSE29272; Supplementary Fig. S5). Taken together, these results reveal that YTHDF1 can activate the Wnt/β-catenin pathway in gastric cancer cells, which is mediated by translational control of FZD7, a key receptor in Wnt/β-catenin signaling.

YTHDF1–FZD7–β-catenin axis contributes to gastric oncogenesis

Driven by the finding that YTHDF1 stimulates the activation of FZD7-β-catenin pathway, we then questioned whether β-catenin

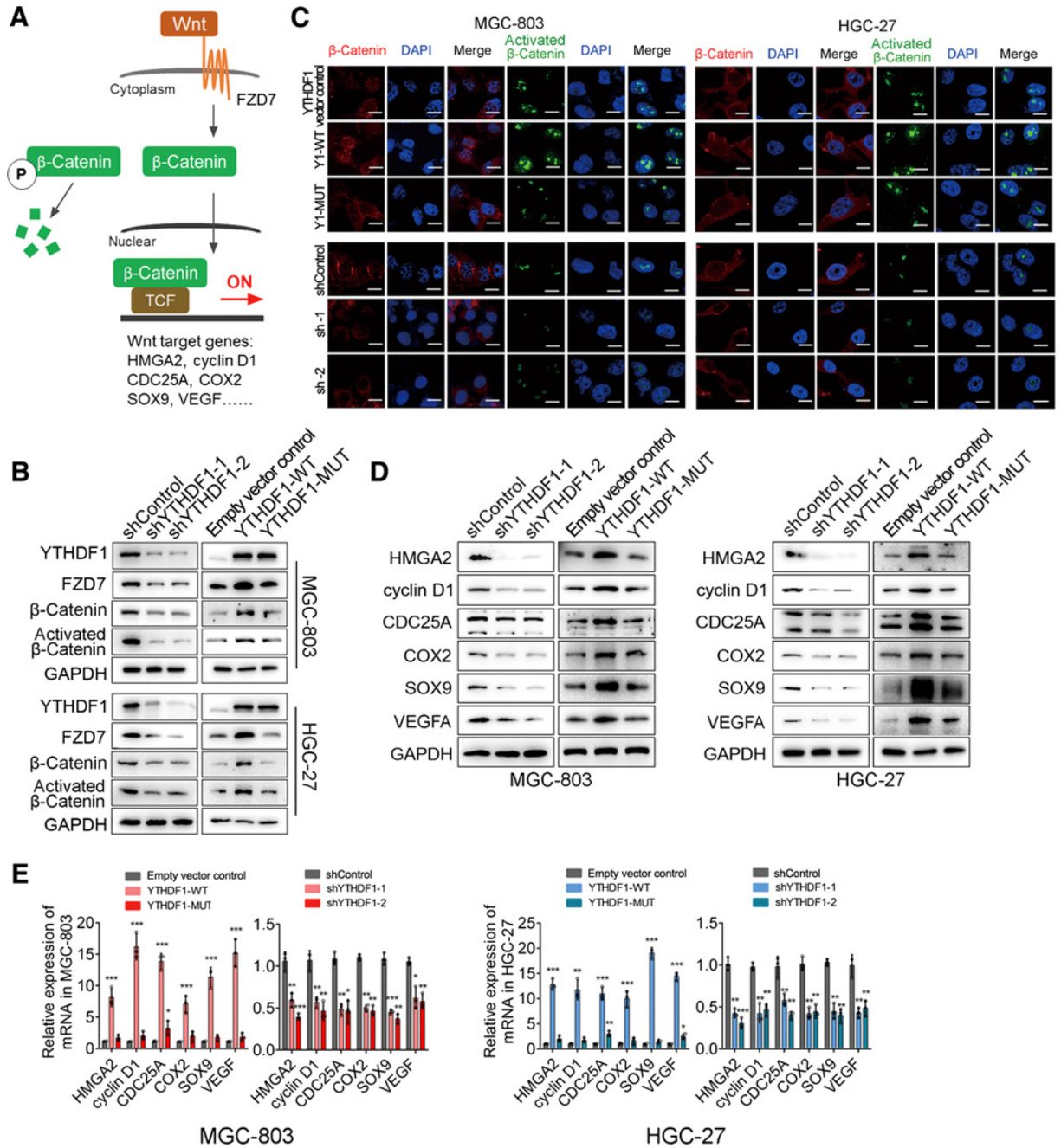

Figure 6.

YTHDF1 regulates the canonical Wnt/β-catenin pathway via FZD7. **A,** Schematic diagram of the canonical Wnt/β-catenin pathway. **B,** Protein level of total (β-catenin) and non-phospho (Ser33/37/Thr41, activated β-catenin) β-catenin in YTHDF1 knockdown or overexpressed MGC-803 and HGC-27 cells. **C,** IF staining analysis of subcellular localization of total (red) and activated (green) β-catenin in YTHDF1 knockdown, overexpressed, or mutant overexpressed MGC-803 and HGC-27 cells. Scale bar, 20 μm. **D,** Immunoblot analysis of β-catenin target genes, HMGA2, cyclin D, CDC25A, COX2, SOX9, and VEGFA in YTHDF1 knockdown, overexpressed or mutant overexpressed MGC-803 and HGC-27 cells. **E,** Quantitative analysis of RNA levels of β-catenin target genes in YTHDF1 knockdown and overexpressed MGC-803 and HGC-27 cells ($n = 3$). *, $P < 0.05$; **, $P < 0.01$; ***, $P < 0.001$ (one-way ANOVA). All data are shown as means ± SD.

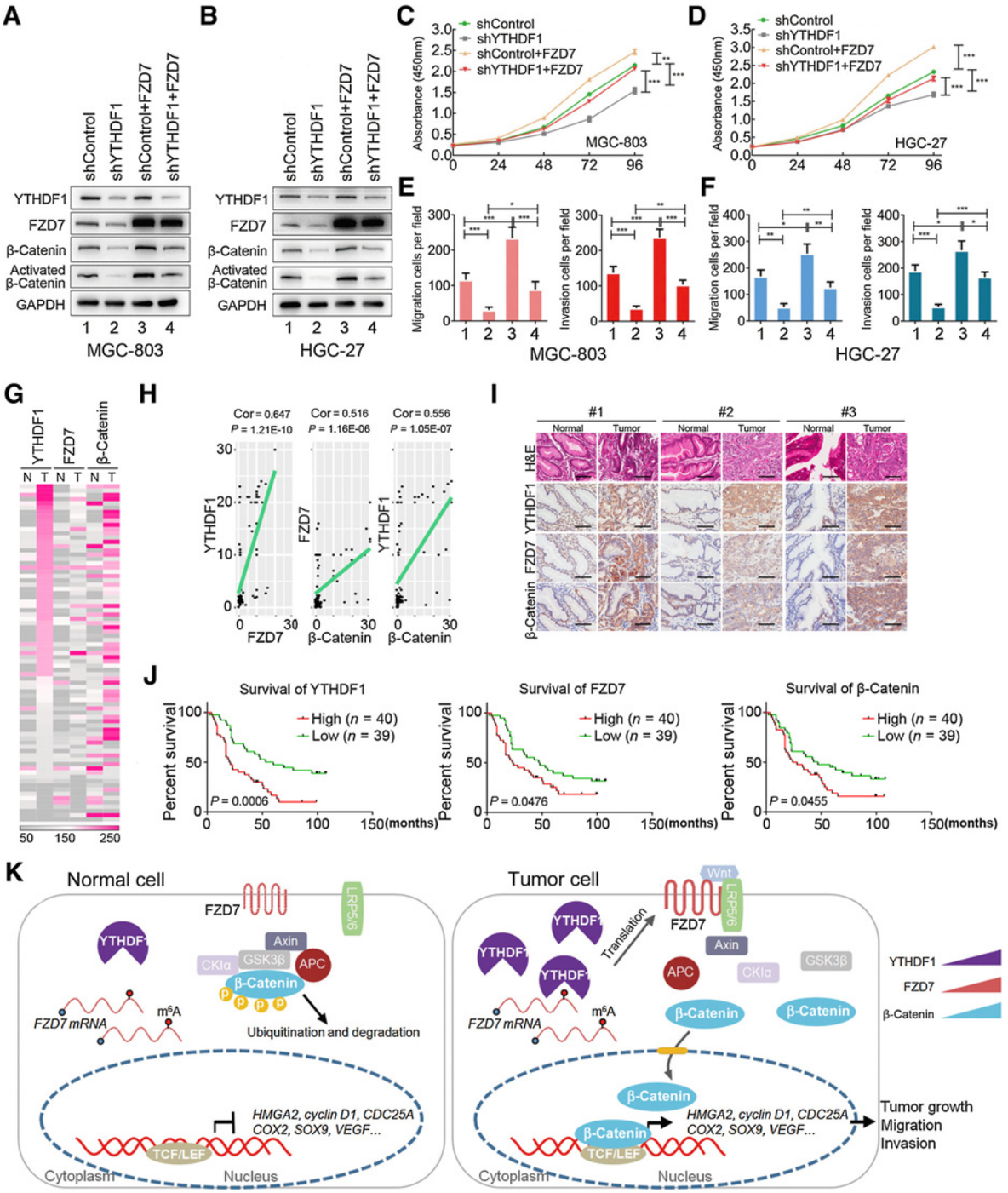

Figure 7.

YTHDF1–FZD7–β-catenin axis promotes gastric cancer progression. **A** and **B,** Western blot analysis of YTHDF1, FZD7, β-catenin, and activated β-catenin in YTHDF1 knockdown MGC-803 (**A**) and HGC-27 (**B**) cells transfected with FZD7 constructs or empty vector control. **C** and **D,** The proliferation of MGC-803 (**C**) and HGC-27 (**D**) cells as described above ($n = 3$). **E,** The migration analysis of MGC-803 (left) and HGC-27 (right) cells as described above ($n = 3$). **F,** The invasion analysis of MGC-803 (left) and HGC-27 (right) cells as described above ($n = 3$). **G,** Heatmap showing IHC chips results of YTHDF1, FZD7, (total) β-catenin expression in human gastric cancer samples ($n = 79$). **H,** The correlation analysis of expressions of YTHDF1, FZD7, and (total) β-catenin in human gastric cancer samples ($n = 79$; Pearson and Spearman correlation test). **I,** Representative IHC chips results of YTHDF1, FZD7, and activated β-catenin in three pairs of gastric tumor and adjacent normal tissues. Scale bar, 100 μm. **J,** Kaplan–Meier survival analysis of YTHDF1, FZD7, and (total) β-catenin (low, $n = 39$ and high, $n = 40$) and overall survival rate of patients with gastric cancer (log-rank with Mantel–Cox test). **K,** Schematic diagram showing how YTHDF1 regulates β-catenin signaling to contribute to gastric tumor progression. *, $P < 0.05$; **, $P < 0.01$; ***, $P < 0.001$ [Student t tests (**H**) or one-way ANOVA (**C, D, E,** and **F**]). All data are shown as means ± SD.

activation could rescue the delayed tumor progression phenotype, which was observed in YTHDF1-deficient gastric cancer cells. Therefore, we used two different approaches either by overexpressing FZD7 (**Fig. 7A** and **B**) or by stimulating β-catenin activity with a specific agonist, SKL2001 (Supplementary Fig. S6A and S6B), which could disrupt the degradation complex and stabilize β-catenin. Similar to previous findings (42, 45), overexpression of FZD7 or activating β-catenin both increased cell proliferation (**Fig. 7C** and **D**; Supplementary Fig. S6C), migration, and invasion (**Fig. 7E** and **F**; Supplementary Fig. S6D–S6G) in YTHDF1-competent MGC803 and HGC-27 cells. Moreover, FZD7 overexpression or SLK2001 treatment in YTHDF1 knockdown cells could reestablished impaired malignant phenotypes to comparable levels as YTHDF1-competent cells. (**Fig. 7C–F**; Supplementary Fig. S6C–S6G). Taken together, the genetic or pharmacologic activation of β-catenin pathway can rescue the decreased proliferation, migration, and invasion induced by YTHDF1 deficiency.

To further investigate whether the changes in protein expression occur in patients' gastric tumor tissues, we performed IHC chips analysis within 79 pairs of in-house human gastric cancer samples and Western blot analysis in 18 pairs of gastric cancer tissues as well as their adjacent normal tissues. As expected, YTHDF1, FZD7, and activated β-catenin showed similar upregulation in human gastric tumors when compared with adjacent normal tissues (**Fig. 7G–I**; Supplementary Fig. S7A–C), which was confirmed in our PDX dataset that inhibition of YTHDF1 also suppressed FZD7 and β-catenin activity (Supplementary Fig. S7D and S7E). Moreover, the Kaplan–Meier survival analysis also indicated that patients with gastric cancer with high YTHDF1, FZD7, β-catenin expression exhibited worse overall survivals [log-rank (Mantel–Cox), YTHDF1, $P = 0.0006$; FZD7, $P = 0.0476$; β-catenin, $P = 0.0455$; **Fig. 7J**], suggesting synchronization changes in YTHDF1, FZD7, and activated β-catenin in gastric tumors represent a reliable prognostic indicator.

To outline our findings, β-catenin is strictly maintained by the protein degradation system in normal gastric mucosa; however, in gastric cancer cells, elevated YTHDF1 activates FZD7 translation and expression, thereby β-catenin is stimulated and translocate to the nucleus to activate the transcription of downstream target genes (**Fig. 7K**). Our data thus uncover a novel YTHDF1–FZD7–β-catenin axis that is critical to regulate cell proliferation and metastasis in gastric cancer development.

Discussion

The m^{6}A has been demonstrated to play important roles in many physiologic and pathologic processes, especially in various tumorigenesis (16). Tumor cells' epi-transcriptome is indeed disrupted by dysregulating m^{6}A-associated writers, readers, and erasers, which modulate m^{6}A establishment, removal, and thus determine modified RNA's fate, respectively (46, 47). Thus, targeting the m^{6}A-associated epi-transcriptome can control the fate of many important transcripts, which might affect distinct aspects of cancer biology (46–52). This approach represents a new strategy for cancer treatment. Clinical trials investigating drugs targeting oncogenic regulators of m^{6}A epi-transcriptome, such as FTO inhibitors Citrate and R-2-hydroxyglutarate (R-2HG) are promising to bring survival advantages in the near future (23, 53).

In this study, we first confirm that as an m^{6}A reader gene, *YTHDF1* is the most frequently mutated m^{6}A-associated gene in gastric tumors. We then show that YTHDF1 is overexpressed in human gastric cancer tissue and plays an essential role in regulating gastric carcinogenesis *in* and *ex vivo*. Given the truth that about 20%–30% of mammalian mRNAs are methylated (54), the increased YTHDF1 expression might have dramatic effects on its targeted transcripts, particularly those involved in cancer development, therefore serves as a key epigenetic regulator. This mechanism probably represents a common oncogenic driver in gastric carcinogenesis, as about 76% (Supplementary Fig. S1B) of patients with gastric cancer exhibited increased YTHDF1 expression.

By integrating the m^{6}A-seq results and transcriptome sequencing results, we discover that the Wnt/β-catenin pathway is an important mediator of YTHDF1's effects on gastric cell proliferation, migration, and invasion. The canonical Wnt/β-catenin pathway plays a crucial role in cell proliferation, cell migration, and homeostasis in normal gastric mucosa (55), but it is also recognized that dysregulation of this pathway is a major driver in the development of gastric cancer, as more than 30% patients with gastric cancer exhibited activated Wnt/β-catenin signaling (55). By using multiple steps screening and validation methods, we further confirm that *FZD7* is a direct target of YTHDF1 and this regulation is m^{6}A dependent. FZD7 is a key receptor on the membrane to relay the Wnt signaling, which is also reported to be frequently overexpressed in human primary gastric cancer tissues and correlated with clinical late-stage and poor survival (42, 43). Thus, our study provides a different angle to target FZD7, which is controlling FZD7's translation via manipulating YTHDF1 or cellular m^{6}A levels. To our knowledge, our study provides direct proof for the first time that the m^{6}A mRNA methylation can regulate Wnt/β-catenin pathway and control gastric cancer progression. Because the dysregulation of Wnt/β-catenin signaling has been implied in multiple human cancers' development (56, 57), our finding might be also applicable to other cancers with increased Wnt/β-catenin activity. Nevertheless, whether YTHDF1 or other m^{6}A regulators play an essential role as in other cancer requires further investigation.

Together, our study demonstrates that the m^{6}A-dependent YTHDF1–FZD7–β-catenin axis plays a crucial role in gastric cancer development. The m^{6}A players, such as YTHDF1, should be further explored as the biomarker for cancer diagnosis, prognostic factors, and ultimately therapeutic targets in various cancers.

Authors' Disclosures

No disclosures were reported.

Authors' Contributions

J. Pi: Data curation, validation, investigation. **W. Wang:** Software, formal analysis. **M. Ji:** Writing–original draft, writing–review and editing. **X. Wang:** Writing–original draft, writing–review and editing. **X. Wei:** Validation, investigation. **J. Jin:** Investigation, writing–review and editing. **T. Liu:** Investigation, writing–review and editing. **J. Qiang:** Software, formal analysis. **Z. Qi:** Investigation. **F. Li:** Investigation. **Y. Liu:** Investigation. **Y. Ma:** Investigation, writing–review and editing. **Y. Si:** Investigation. **Y. Huo:** Software, formal analysis. **Y. Gao:** Software, formal analysis. **Y. Chen:** Investigation. **L. Dong:** Software, formal analysis. **R. Su:** Investigation. **J. Chen:** Writing–review and editing. **S. Rao:** Writing–review and editing. **P. Yi:** Writing–review and editing. **S. Yu:** Writing–review and editing. **F. Wang:** Supervision, project administration, writing–review and editing. **J. Yu:** Conceptualization, supervision, project administration, writing–review and editing.

Acknowledgments

This research was supported by the National Natural Science Foundation of China (81530007, 81970103, and 31725013), CAMS Innovation Fund for Medical Sciences (2017-I2M-3-009, 2017-I2M-1-015, and 2019-I2M-2-001), CAMS Young Talents Award Program (2018RC310013), the National Key Research and Development

Program of China (2016YFA0100601), the National Key Basic Research Program of China (2015CB943001), the CAMS (2017-I2M-B&R-04), and grant from Medical Epigenetics Research Center, CAMS (2017PT31035).

The authors owe their thanks to the patients. The authors are grateful to Cancer Institute and Hospital, Chinese Academy of Medical Sciences and Shanxi Cancer Hospital.

The costs of publication of this article were defrayed in part by the payment of page charges. This article must therefore be hereby marked *advertisement* in accordance with 18 U.S.C. Section 1734 solely to indicate this fact.

Received January 10, 2020; revised April 8, 2020; accepted August 6, 2020; published first August 11, 2020.

References

1. Roundtree IA, Evans ME, Pan T, He C. Dynamic RNA modifications in gene expression regulation. Cell 2017;169:1187–200.
2. Zhong S, Li H, Bodi Z, Button J, Vespa L, Herzog M, et al. MTA is an Arabidopsis messenger RNA adenosine methylase and interacts with a homolog of a sex-specific splicing factor. Plant Cell 2008;20:1278–88.
3. Desrosiers R, Friderici K, Rottman F. Identification of methylated nucleosides in messenger RNA from Novikoff hepatoma cells. Proc Natl Acad Sci U S A 1974; 71:3971–5.
4. Furuichi Y, Shatkin AJ, Stavnezer E, Bishop JM. Blocked, methylated 5'-terminal sequence in avian sarcoma virus RNA. Nature 1975;257:618–20.
5. Kowalak JA, Dalluge JJ, McCloskey JA, Stetter KO. The role of posttranscriptional modification in stabilization of transfer RNA from hyperthermophiles. Biochemistry 1994;33:7869–76.
6. Deng X, Chen K, Luo GZ, Weng X, Ji Q, Zhou T, et al. Widespread occurrence of N6-methyladenosine in bacterial mRNA. Nucleic Acids Res 2015;43:6557–67.
7. Krug RM, Morgan MA, Shatkin AJ. Influenza viral mRNA contains internal N6-methyladenosine and 5'-terminal 7-methylguanosine in cap structures. J Virol 1976;20:45–53.
8. Jia G, Fu Y, Zhao X, Dai Q, Zheng G, Yang Y, et al. N6-methyladenosine in nuclear RNA is a major substrate of the obesity-associated FTO. Nat Chem Biol 2011;7:885–7.
9. Zheng G, Dahl JA, Niu Y, Fedorcsak P, Huang CM, Li CJ, et al. ALKBH5 is a mammalian RNA demethylase that impacts RNA metabolism and mouse fertility. Mol Cell 2013;49:18–29.
10. Liu J, Yue Y, Han D, Wang X, Fu Y, Zhang L, et al. A METTL3-METTL14 complex mediates mammalian nuclear RNA N6-adenosine methylation. Nat Chem Biol 2014;10:93–5.
11. Pendleton KE, Chen B, Liu K, Hunter OV, Xie Y, Tu BP, et al. The U6 snRNA m(6)A methyltransferase METTL16 regulates SAM synthetase intron retention. Cell 2017;169:824–35.e14.
12. Mendel M, Chen KM, Homolka D, Gos P, Pandey RR, McCarthy AA, et al. Methylation of structured RNA by the m(6)A writer METTL16 is essential for mouse embryonic development. Mol Cell 2018;71:986–1000.e11.
13. Patil DP, Pickering BF, Jaffrey SR. Reading m(6)A in the transcriptome: m(6)A-binding proteins. Trends Cell Biol 2018;28:113–27.
14. Wang X, Zhao BS, Roundtree IA, Lu Z, Han D, Ma H, et al. N(6)-methyladenosine modulates messenger RNA translation efficiency. Cell 2015;161:1388–99.
15. Huang H, Weng H, Sun W, Qin X, Shi H, Wu H, et al. Recognition of RNA N(6)-methyladenosine by IGF2BP proteins enhances mRNA stability and translation. Nat Cell Biol 2018;20:285–95.
16. Fu Y, Dominissini D, Rechavi G, He C. Gene expression regulation mediated through reversible m(6)A RNA methylation. Nat Rev Genet 2014;15:293–306.
17. Wojtas MN, Pandey RR, Mendel M, Homolka D, Sachidanandam R, Pillai RS. Regulation of m(6)A transcripts by the 3'→5' RNA helicase YTHDC2 is essential for a successful meiotic program in the mammalian germline. Mol Cell 2017;68: 374–87.e12.
18. Xiao W, Adhikari S, Dahal U, Chen YS, Hao YJ, Sun BF, et al. Nuclear m(6)A reader YTHDC1 regulates mRNA splicing. Mol Cell 2016;61:507–19.
19. Alarcon CR, Goodarzi H, Lee H, Liu X, Tavazoie S, Tavazoie SF. HNRNPA2B1 Is a mediator of m(6)A-dependent nuclear rna processing events. Cell 2015;162: 1299–308.
20. Meng TG, Lu X, Guo L, Hou GM, Ma XS, Li QN, et al. Mettl14 is required for mouse postimplantation development by facilitating epiblast maturation. FASEB J 2019;33:1179–87.
21. Zhao BS, Wang X, Beadell AV, Lu Z, Shi H, Kuuspalu A, et al. m(6)A-dependent maternal mRNA clearance facilitates zebrafish maternal-to-zygotic transition. Nature 2017;542:475–8.
22. Weng H, Huang H, Wu H, Qin X, Zhao BS, Dong L, et al. METTL14 inhibits hematopoietic stem/progenitor differentiation and promotes leukemogenesis via mRNA m(6)A modification. Cell stem cell 2018;22:191–205.e9.
23. Su R, Dong L, Li C, Nachtergaele S, Wunderlich M, Qing Y, et al. R-2HG exhibits anti-tumor activity by targeting FTO/m(6)A/MYC/CEBPA signaling. Cell 2018; 172:90–105.e23.
24. Cui Q, Shi H, Ye P, Li L, Qu Q, Sun G, et al. m(6)A RNA methylation regulates the self-renewal and tumorigenesis of glioblastoma stem cells. Cell Rep 2017;18: 2622–34.
25. Vu LP, Pickering BF, Cheng Y, Zaccara S, Nguyen D, Minuesa G, et al. The N(6)-methyladenosine (m(6)A)-forming enzyme METTL3 controls myeloid differentiation of normal hematopoietic and leukemia cells. Nat Med 2017; 23:1369–76.
26. Li Z, Weng H, Su R, Weng X, Zuo Z, Li C, et al. FTO plays an oncogenic role in acute myeloid leukemia as a N(6)-methyladenosine rna demethylase. Cancer Cell 2017;31:127–41.
27. Ma JZ, Yang F, Zhou CC, Liu F, Yuan JH, Wang F, et al. METTL14 suppresses the metastatic potential of hepatocellular carcinoma by modulating N(6)-methyladenosine-dependent primary MicroRNA processing. Hepatology 2017;65:529–43.
28. Carruthers RD, Ahmed SU, Ramachandran S, Strathdee K, Kurian KM, Hedley A, et al. Replication stress drives constitutive activation of the DNA damage response and radioresistance in glioblastoma stem-like cells. Cancer Res 2018;78: 5060–71.
29. Lu J, Guo H, Treekitkarnmongkol W, Li P, Zhang J, Shi B, et al. 14-3-3zeta cooperates with ErbB2 to promote ductal carcinoma *in situ* progression to invasive breast cancer by inducing epithelial-mesenchymal transition. Cancer Cell 2009;16:195–207.
30. Kashima K, Watanabe M, Satoh Y, Hata J, Ishii N, Aoki Y. Inhibition of lymphatic metastasis in neuroblastoma by a novel neutralizing antibody to vascular endothelial growth factor-D. Cancer Sci 2012;103:2144–52.
31. Van Nostrand EL, Pratt GA, Shishkin AA, Gelboin-Burkhart C, Fang MY, Sundararaman B, et al. Robust transcriptome-wide discovery of RNA-binding protein binding sites with enhanced CLIP (eCLIP). Nat Methods 2016;13:508–14.
32. Kim D, Pertea G, Trapnell C, Pimentel H, Kelley R, Salzberg SL. TopHat2: accurate alignment of transcriptomes in the presence of insertions, deletions and gene fusions. Genome Biol 2013;14:R36.
33. Dominissini D, Moshitch-Moshkovitz S, Salmon-Divon M, Amariglio N, Rechavi G. Transcriptome-wide mapping of N(6)-methyladenosine by m(6) A-seq based on immunocapturing and massively parallel sequencing. Nat Protoc 2013;8:176–89.
34. Huang da W, Sherman BT, Lempicki RA. Systematic and integrative analysis of large gene lists using DAVID bioinformatics resources. Nat Protoc 2009;4:44–57.
35. Huang da W, Sherman BT, Lempicki RA. Bioinformatics enrichment tools: paths toward the comprehensive functional analysis of large gene lists. Nucleic Acids Res 2009;37:1–13.
36. Wang Y, Song F, Zhu J, Zhang S, Yang Y, Chen T, et al. GSA: genome sequence archive. Genomics Proteomics Bioinformatics 2017;15:14–8.
37. BIG Data Center Members. Database resources of the BIG data center in 2018. Nucleic Acids Res 2018;46:D14–20.
38. Wang K, Yuen ST, Xu J, Lee SP, Yan HH, Shi ST, et al. Whole-genome sequencing and comprehensive molecular profiling identify new driver mutations in gastric cancer. Nat Genet 2014;46:573–82.
39. Cerami E, Gao J, Dogrusoz U, Gross BE, Sumer SO, Aksoy BA, et al. The cBio cancer genomics portal: an open platform for exploring multidimensional cancer genomics data. Cancer Discov 2012;2:401–4.
40. Kakiuchi M, Nishizawa T, Ueda H, Gotoh K, Tanaka A, Hayashi A, et al. Recurrent gain-of-function mutations of RHOA in diffuse-type gastric carcinoma. Nat Genet 2014;46:583–7.
41. Wang K, Kan J, Yuen ST, Shi ST, Chu KM, Law S, et al. Exome sequencing identifies frequent mutation of ARID1A in molecular subtypes of gastric cancer. Nat Genet 2011;43:1219–23.

42. Li G, Su Q, Liu H, Wang D, Zhang W, Lu Z, et al. Frizzled7 promotes epithelial-to-mesenchymal transition and stemness via activating canonical wnt/beta-catenin pathway in gastric cancer. Int J Biol Sci 2018;14:280–93.
43. Kirikoshi H, Sekihara H, Katoh M. Up-regulation of Frizzled-7 (FZD7) in human gastric cancer. Int J Oncol 2001;19:111–5.
44. Xu C, Liu K, Ahmed H, Loppnau P, Schapira M, Min J. Structural basis for the discriminative recognition of n6-methyladenosine RNA by the human YT521-B homology domain family of proteins. J Biol Chem 2015;290:24902–13.
45. Deng YZ, Yao F, Li JJ, Mao ZF, Hu PT, Long LY, et al. RACK1 suppresses gastric tumorigenesis by stabilizing the beta-catenin destruction complex. Gastroenterology 2012;142:812–23.e15.
46. Lobo J, Barros-Silva D, Henrique R, Jeronimo C. The emerging role of epitranscriptomics in cancer: focus on urological tumors. Genes 2018;9:552.
47. Jaffrey SR, Kharas MG. Emerging links between m(6)A and misregulated mRNA methylation in cancer. Genome Med 2017;9:2.
48. Zhang C, Samanta D, Lu H, Bullen JW, Zhang H, Chen I, et al. Hypoxia induces the breast cancer stem cell phenotype by HIF-dependent and ALKBH5-mediated m(6)A-demethylation of NANOG mRNA. Proc Natl Acad Sci U S A 2016; 113:E2047–56.
49. Lin S, Choe J, Du P, Triboulet R, Gregory RI. The m(6)A methyltransferase METTL3 promotes translation in human cancer cells. Mol Cell 2016; 62:335–45.
50. Chen M, Wei L, Law CT, Tsang FH, Shen J, Cheng CL, et al. RNA N6-methyladenosine methyltransferase-like 3 promotes liver cancer progression through YTHDF2-dependent posttranscriptional silencing of SOCS2. Hepatology 2018;67:2254–70.
51. Liu J, Eckert MA, Harada BT, Liu SM, Lu Z, Yu K, et al. m(6)A mRNA methylation regulates AKT activity to promote the proliferation and tumorigenicity of endometrial cancer. Nat Cell Biol 2018;20:1074–83.
52. Zhang S, Zhao BS, Zhou A, Lin K, Zheng S, Lu Z, et al. m(6)A demethylase ALKBH5 maintains tumorigenicity of glioblastoma stem-like cells by sustaining FOXM1 expression and cell proliferation program. Cancer Cell 2017; 31:591–606.e6.
53. Tusup M, Kundig T, Pascolo S. Epitranscriptomics of cancer. World J Clin Oncol 2018;9:42–55.
54. Dominissini D, Moshitch-Moshkovitz S, Schwartz S, Salmon-Divon M, Ungar L, Osenberg S, et al. Topology of the human and mouse m6A RNA methylomes revealed by m6A-seq. Nature 2012;485:201–6.
55. Chiurillo MA. Role of the Wnt/beta-catenin pathway in gastric cancer: an in-depth literature review. World J Exp Med 2015;5:84–102.
56. Clevers H, Nusse R. Wnt/beta-catenin signaling and disease. Cell 2012;149: 1192–205.
57. Klaus A, Birchmeier W. Wnt signalling and its impact on development and cancer. Nat Rev Cancer 2008;8:387–98.